Science Advances
AAAS

Supplementary Materials for

Insights into complex I assembly: Function of NDUFAF1 and a link with cardiolipin remodeling

Jonathan Schiller *et al.*

Corresponding author: Janet Vonck, janet.vonck@biophys.mpg.de;
Volker Zickermann, zickermann@med.uni-frankfurt.de

Sci. Adv. **8**, eadd3855 (2022)
DOI: 10.1126/sciadv.add3855

The PDF file includes:

Other Supplementary Material for this manuscript includes the following:

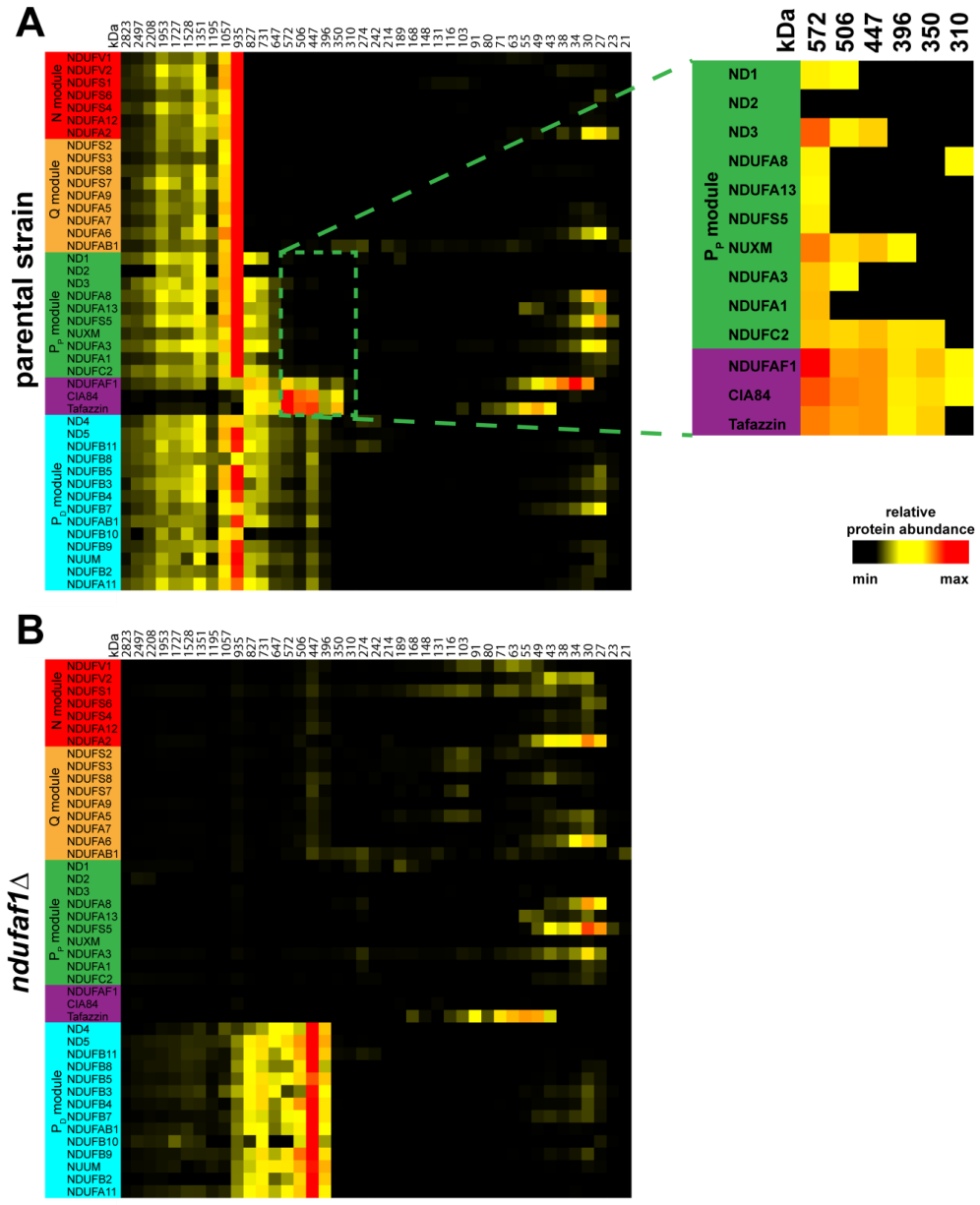

Fig. S1. Complexome profiling of intact mitochondria and protein purification. Section of complexome profiling analysis of mitochondria from parental and *ndufaf1*Δ strains with migration profiles of NDUFAF1, CIA84 and tafazzin and complex I subunits assigned to the N, Q, P_P and P_D modules. Relative abundance of proteins identified and quantified in gel slices using LC–ESI mass spectrometry is represented as a heat map. Note that ND4L and ND6 were not detected and ND2 and ND3 produced weak signals because they are highly hydrophobic and lack suitable cleavage sites. OXPHOS complexes of bovine heart mitochondria were used for mass calibration. **(A)** Complexome profile of the parental strain. The inset shows a magnification of the area highlighted by a dotted rectangle; the heat map was adjusted to visualize signals of assembly intermediates that are orders of magnitude weaker than signals for mature complex I. **(B)** Section of complexome profile of the *ndufaf1*Δ deletion strain.

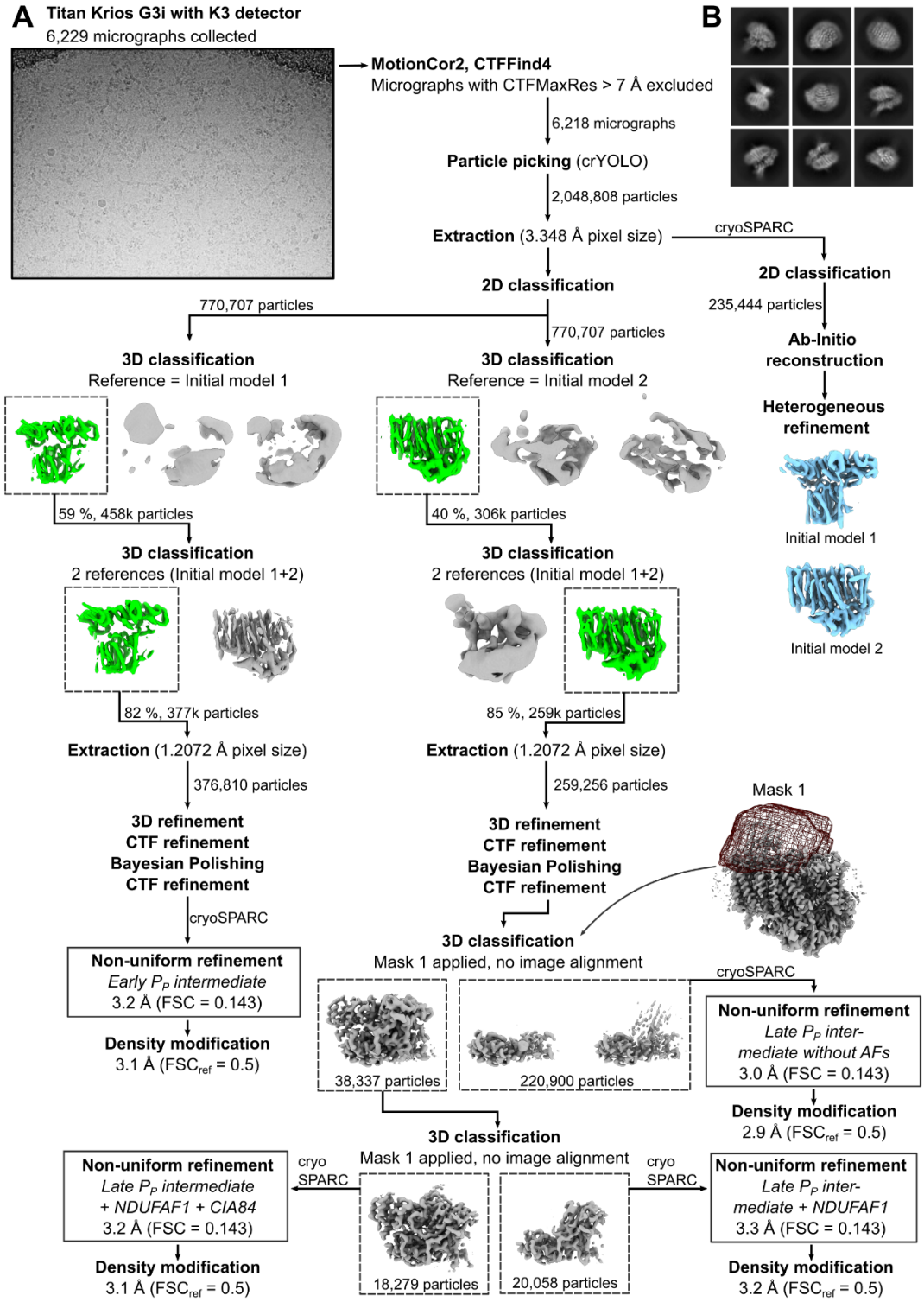

Fig. S2. Processing pipeline of the cryo-EM dataset. (A) Representative micrograph and workflow of single-particle processing of the dataset of complex I assembly intermediates. Data was processed in RELION4 or if specified, in cryoSPARC. Density modification was performed with *phenix.resolve_cryo_em*. **(B)** Representative 2D class averages from 2D classification in cryoSPARC.

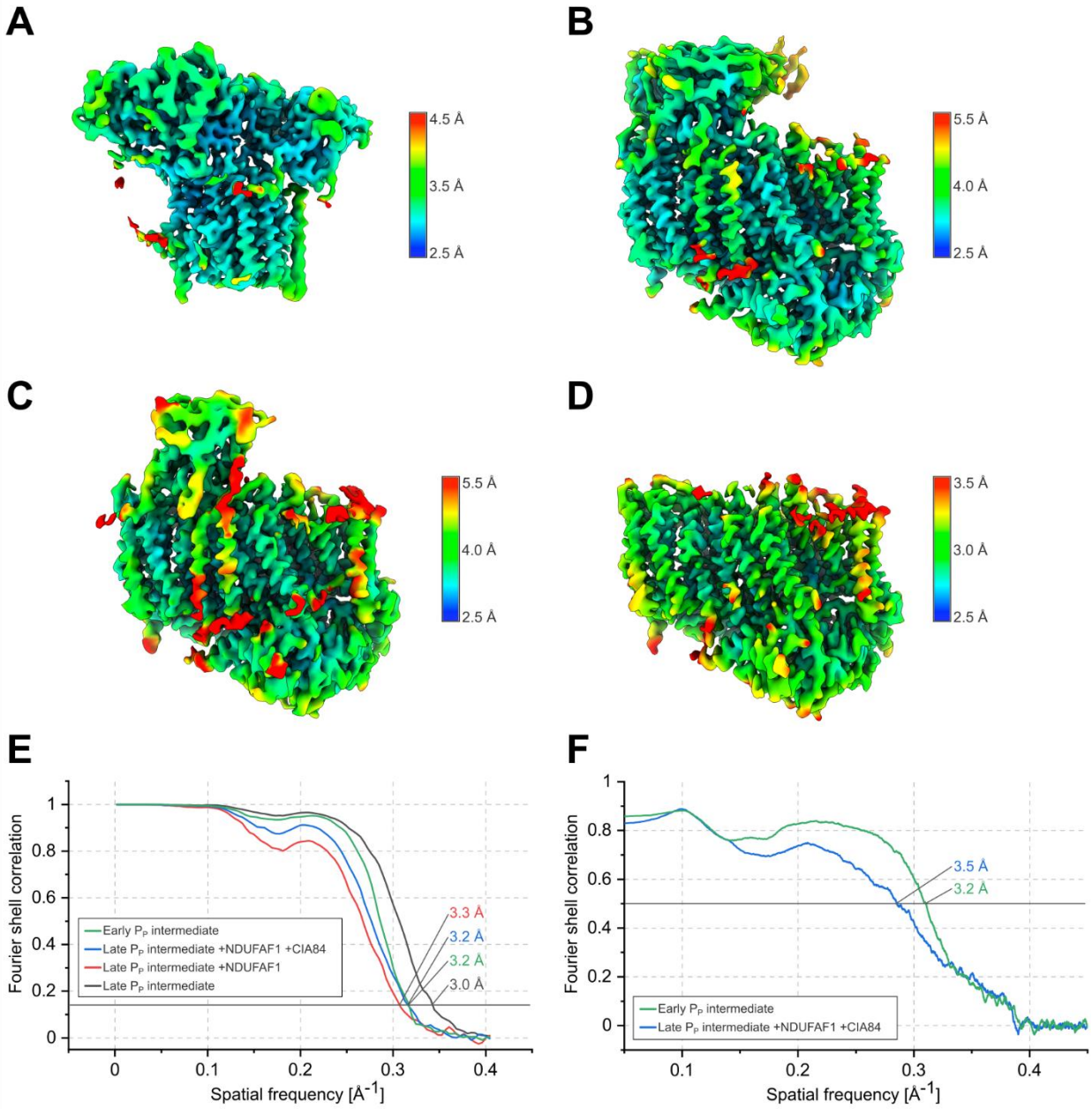

Fig. S3. Cryo-EM density maps of complex I assembly intermediates. Local resolution (threshold for local FSC=0.5) of **(A)** the early P_P module intermediate, **(B)** the late P_P module intermediate with NDUFAF1 and CIA84 bound, **(C)** with only NDUFAF1 bound and **(D)** without assembly factors bound. **(E)** Two-halfmap Fourier shell correlation curves. **(F)** Map to model Fourier shell correlation curves.

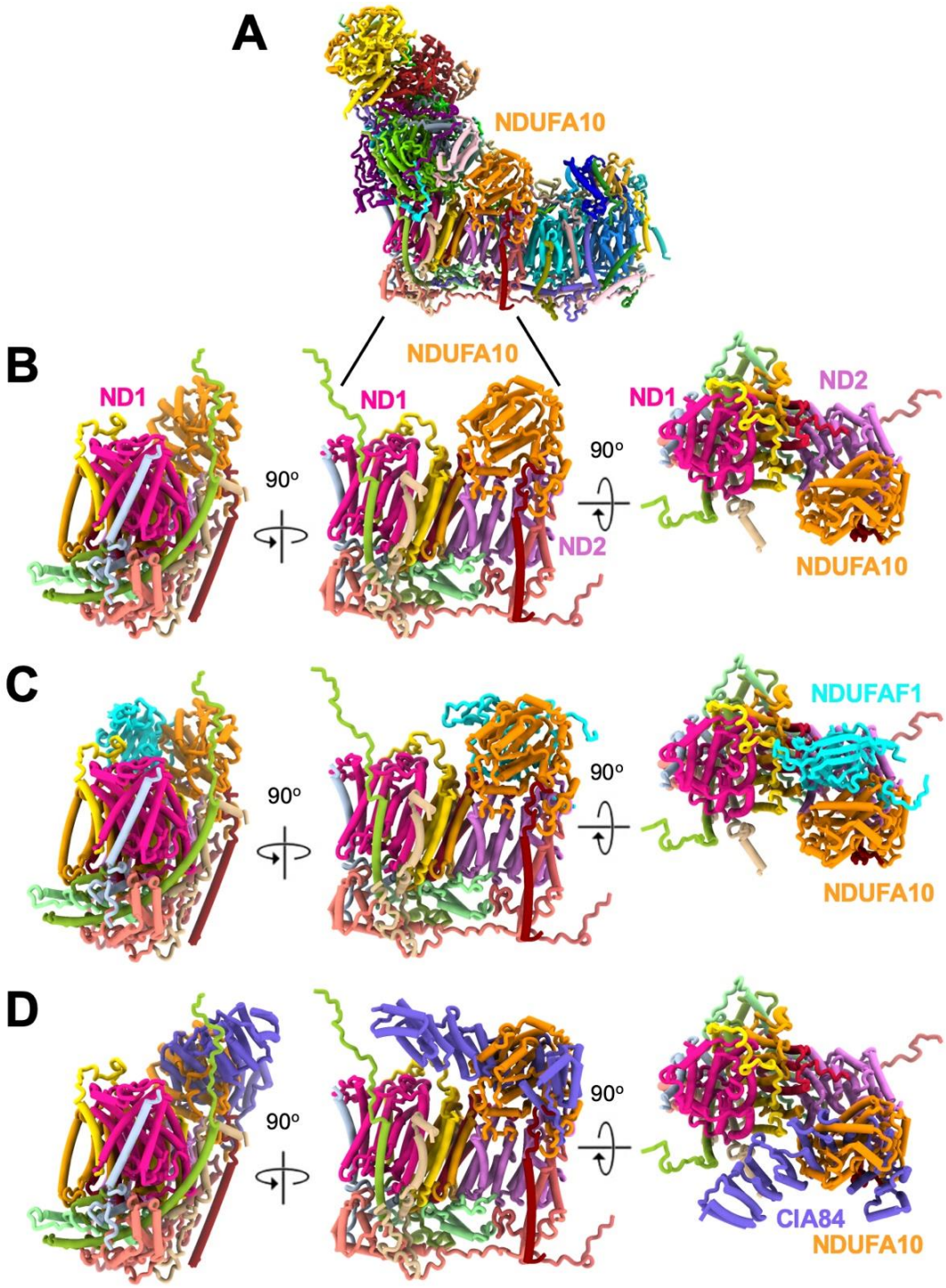

Fig. S4. Assembly factors and mammalian complex I. (A) Mouse complex I (pdb 6g2j) (*48*) contains the accessory subunit NDUFA10 (orange) specific for metazoa. **(B)** The P_P module of mouse complex I in three orientations: same view as (A) (middle), seen from the back (left) and seen from the matrix (right). **(C)** As (B) overlaid with *Y. lipolytica* NDUFAF1 (cyan), fitted by alignment of ND2. NDUFAF1 and NDUFA10 do not overlap, consistent with a binding mode of the assembly factor. **(D)** *Y. lipolytica* CIA84 (purple) binds to ND2 at the same position as NDUFA10 (orange) in metazoa.

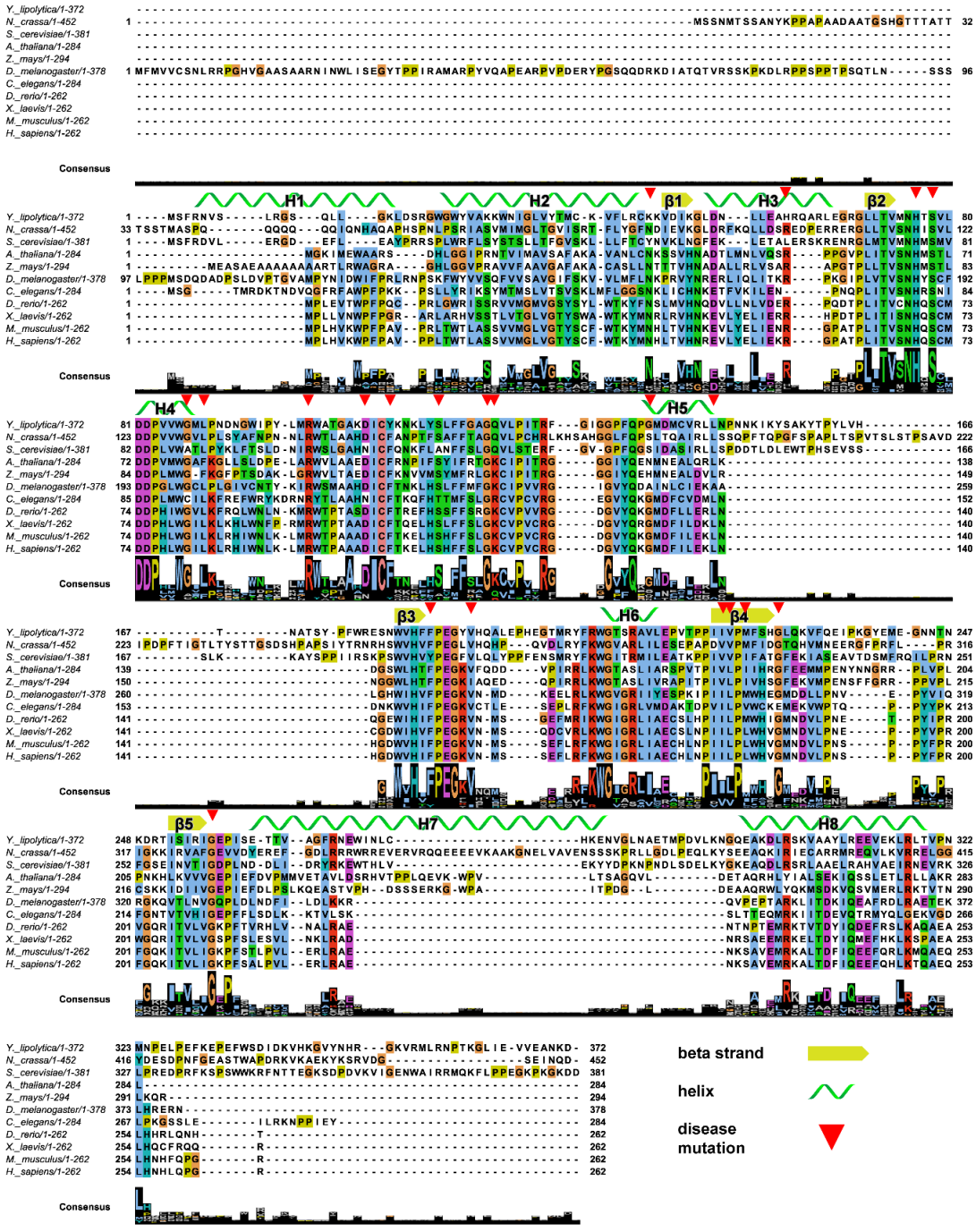

Fig. S5. Tafazzin sequence alignment and disease mutants. Sequence IDs used in this alignment: Q16635-3 *H. sapiens*, Q91WF0 *M. musculus*, A0A1L8F5D6 *X. laevis*, Q9V6G5 *D. melanogaster*, Q06510 *S. cerevisiae*, F1QCP6 *D. rerio*, Q23598 *C. elegans*, Q6CBZ7 *Y. lipolytica*, A0A0B0DLI6 *N. crassa*, Q9ZV87 *A. thaliana* and A0A1D6JHG4 *Z. mays*. Disease mutants are listed according to (*55*).

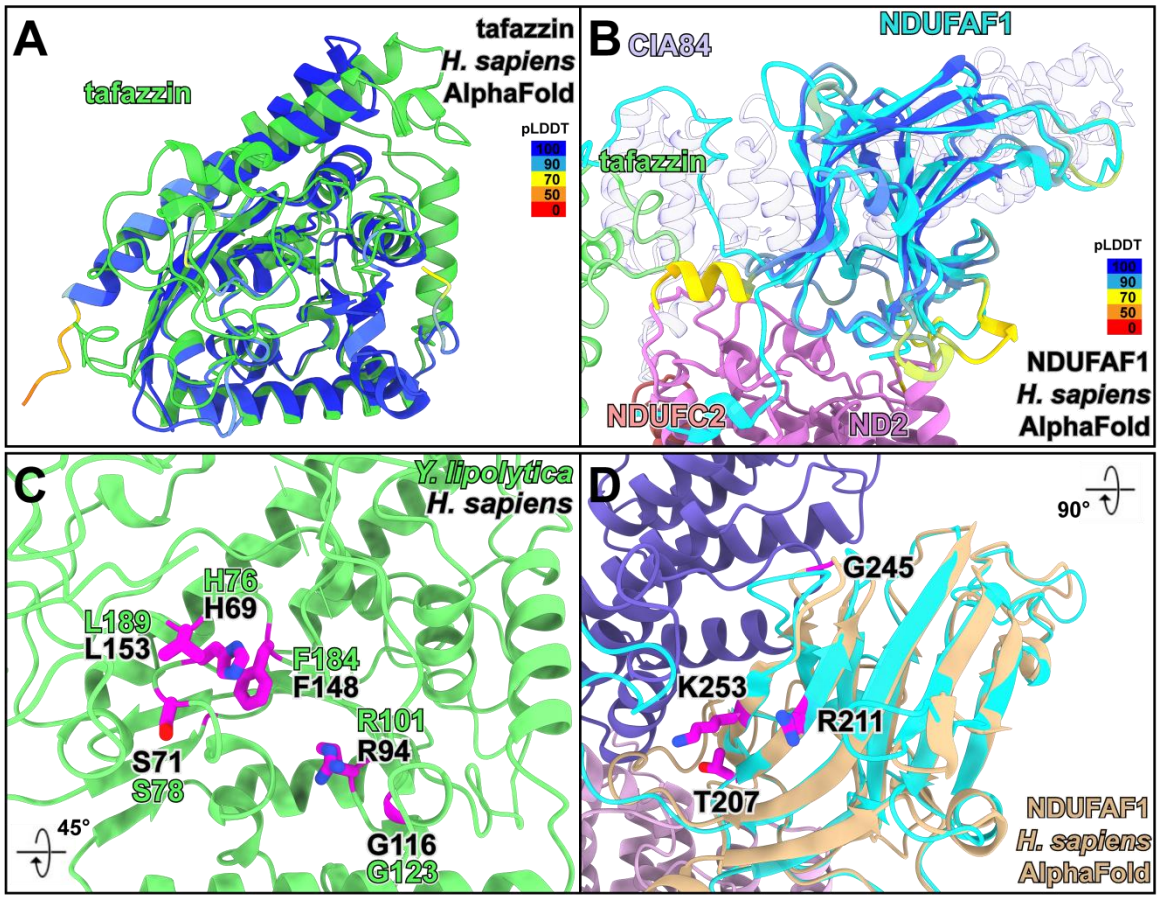

Fig. S6. Pathogenic mutations in tafazzin and NDUFAF1. Overlay of cryo-EM structures of **(A)** tafazzin and **(B)** NDUFAF1 (colors as in Fig. 1) with AlphaFold models of their *H. sapiens* orthologues. The AlphaFold models are colored based on the pLDDT (predicted Local Distance Difference Test) confidence score; sequence stretches of NDUFAF1 with low pLDDT score (residues 1-111) are not shown. **(C)** *Y. lipolytica* tafazzin with conserved residues of which exchanges are known to cause Barth syndrome in humans (stick representation, magenta; residue numbers in black, human; green, corresponding residue in *Y. lipolytica*). (D) Residues of human NDUFAF1 (stick representation, magenta) of which mutations were described to cause disease (T207P, R211C, G245R, K253R, V252_K253del) (*21*, *22*).

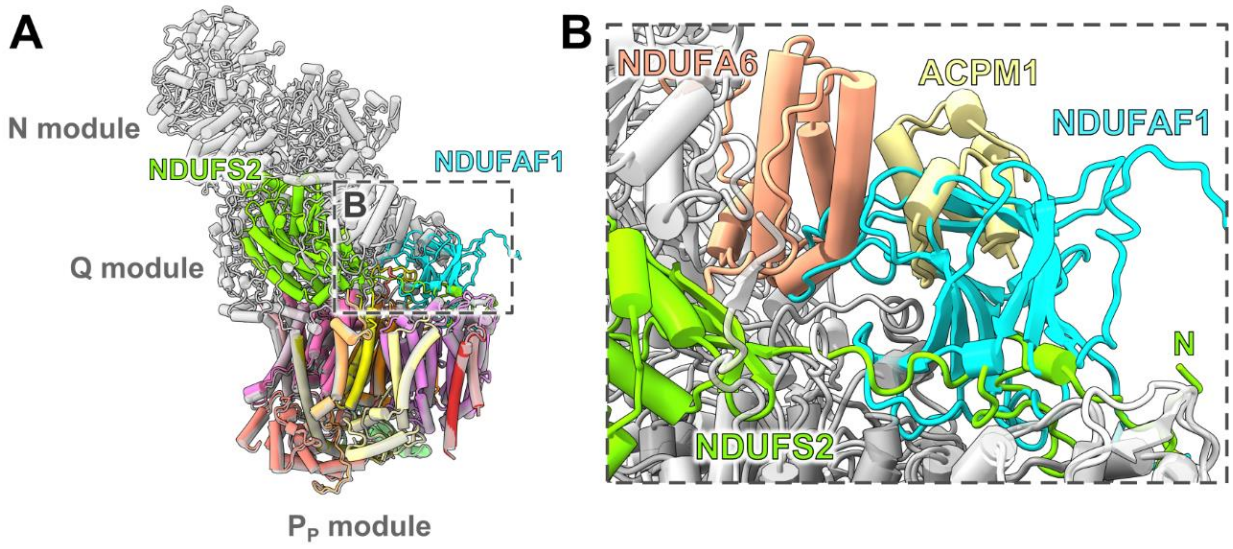

Fig. S7. Overlap of assembly factor NDUFAF1 with the position of the Q module. (A) Side view of the late P_P module intermediate (colored by subunit) and of mature *Y. lipolytica* complex I without P_D module (pdb 7o71, colored grey except for NDUFS2). **(B)** The long N-terminal loop of Q module subunit NDUFS2 clashes with NDUFAF1 and can only fold into its native conformation after NDUFAF1 dissociation. As accessory subunit NDUFA6 and ACPM1 also collide with NDUFAF1, dissociation of the assembly factor must occur before binding of these two subunits to the Q module.

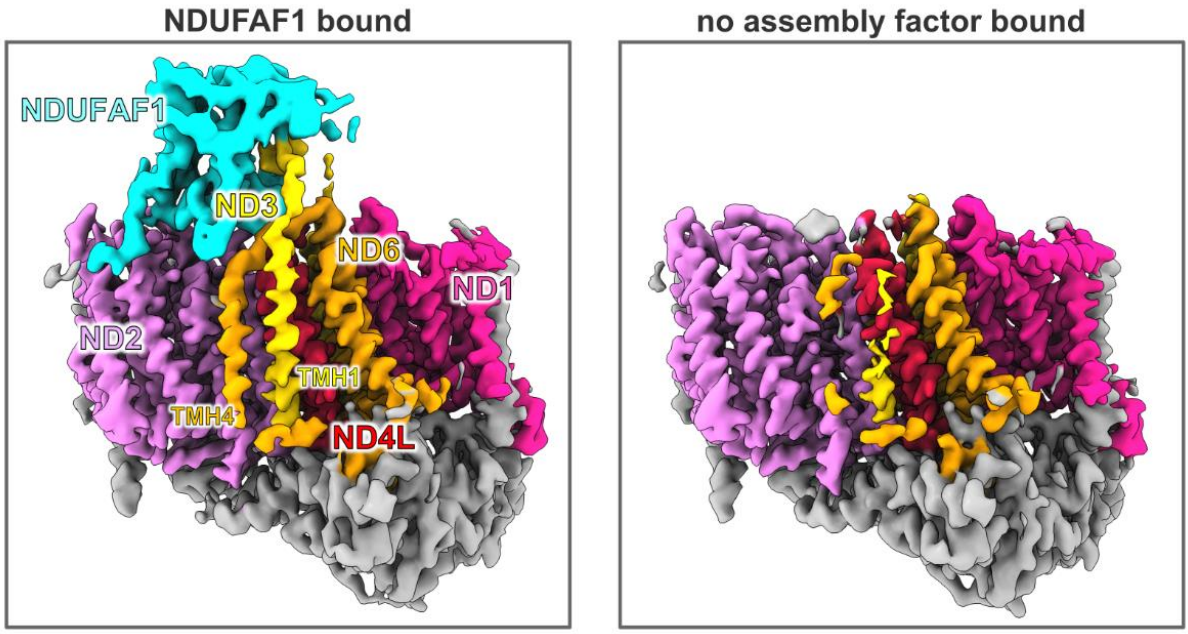

Fig. S8. NDUFAF1 maintains integrity of ND3 and ND6 in the late P_P module intermediate. 3D maps of the late P_P module intermediate with NDUFAF1 bound (left) and without any assembly factor bound (right) at 6 σ contour levels. Without NDUFAF1 bound, map density for $TMH1^{ND3}$ and for $TMH4^{ND6}$ is substantially decreased, indicating a dissociation/unfolding of these helices. Map colored according to core subunits and NDUFAF1.

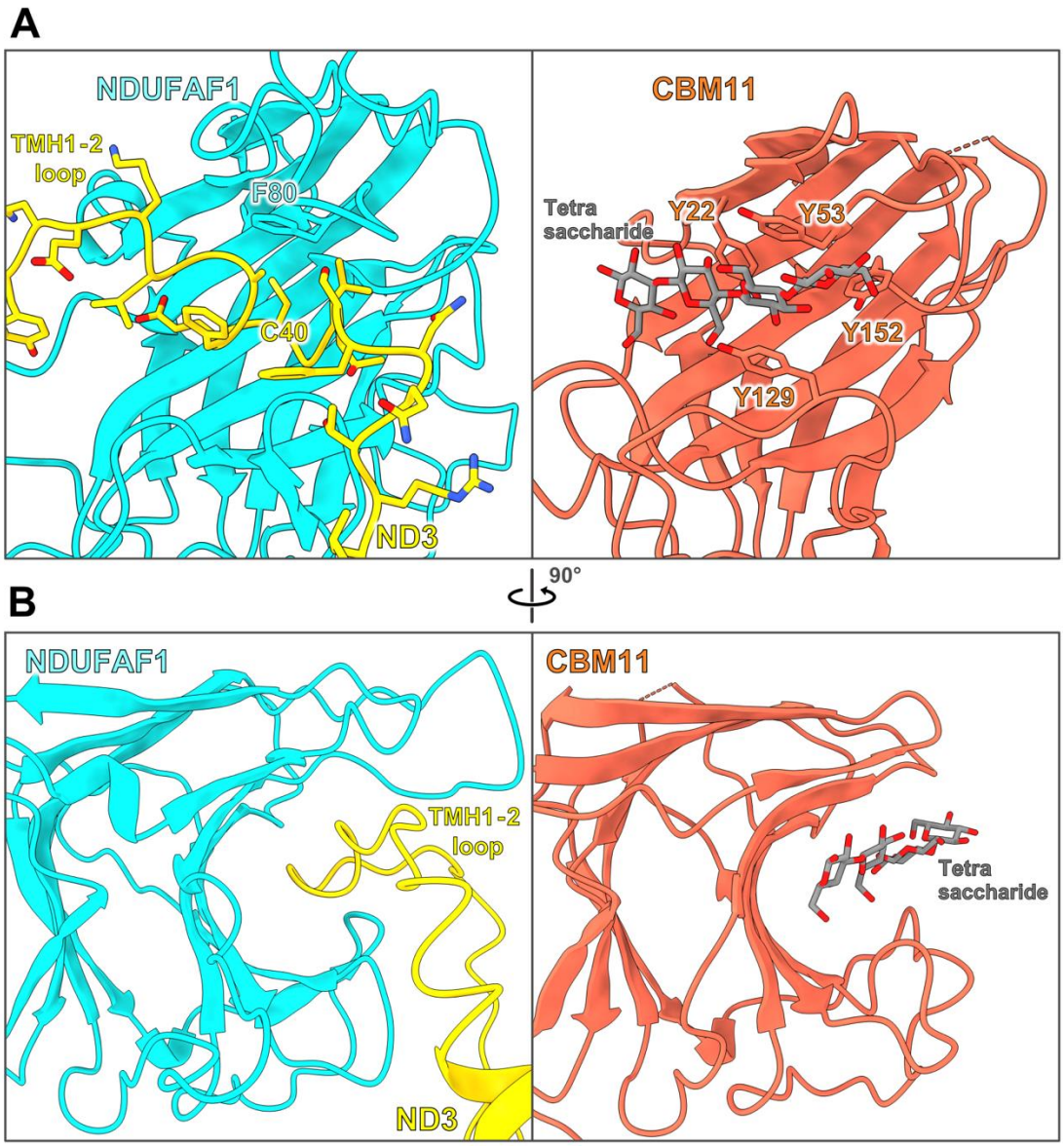

Fig. S9. Structural similarity between NDUFAF1 and family 11 CBM. (A) Structures of assembly factor NDUFAF1 (left) and of CBM11 (right, pdb 6r3m) bound to the TMH1-2 loop of ND3 and a tetrasaccharide, respectively. The 3D structures of NDUFAF1 and CBM11 are very similar; however, residue conservation in the binding cleft is weak. None of the four tyrosines of CBM11, crucial for substrate binding, is present in NDUFAF1. An aromatic residue is conserved in NDUFAF1 (Phe80 in *Y. lipolytica*), which binds to a hydrophobic segment of the TMH1-2 loop of ND3 near $Cys40^{ND3}$. **(B)** In both NDUFAF1 and CBM11, the binding cleft is formed by a concave β-sandwich.

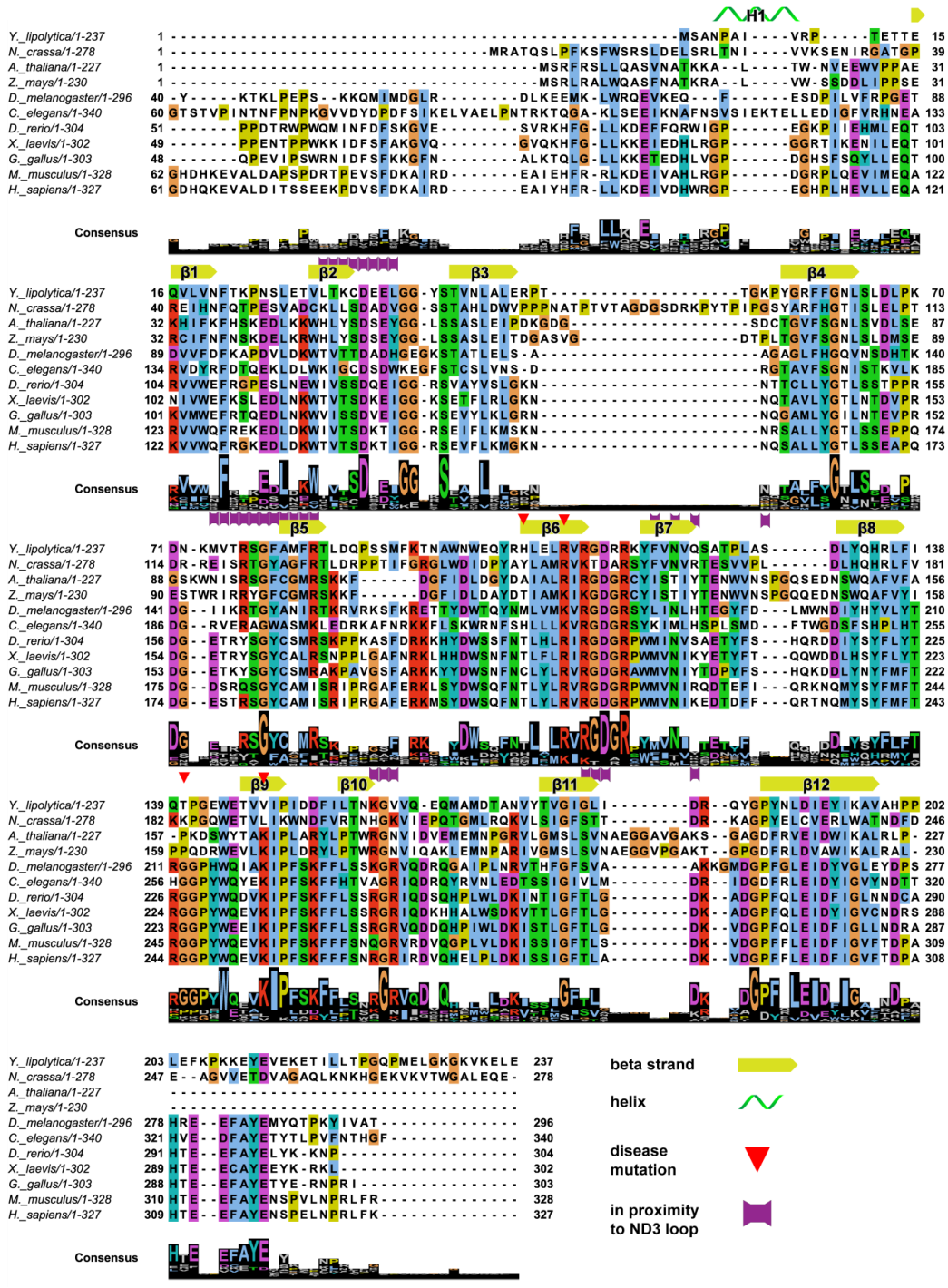

Fig. S10. Sequence alignment of NDUFAF1. N-terminal sequences showing no conservation were excluded for space reasons. Sequence IDs used in this alignment: Q9Y375 *H. sapiens*, Q9CWX2 *M. musculus*, A0A1L8FB53 *X. laevis*, Q9VAI1 *D. melanogaster*, E1BZH1 *G. gallus*, Q5CZW0 *D. rerio*, Q18726 *C. elegans*, Q6C935 *Y. lipolytica*, A0A0B0DI31 *N. crassa*, Q9LQI7 *A. thaliana* and B6STL4 *Z. mays*. Purple polygons indicate residues in proximity (<6 Å) to the loop between helices 1 and 2 of ND3 (fig. S11). Disease mutations as described in *(21,22)*.

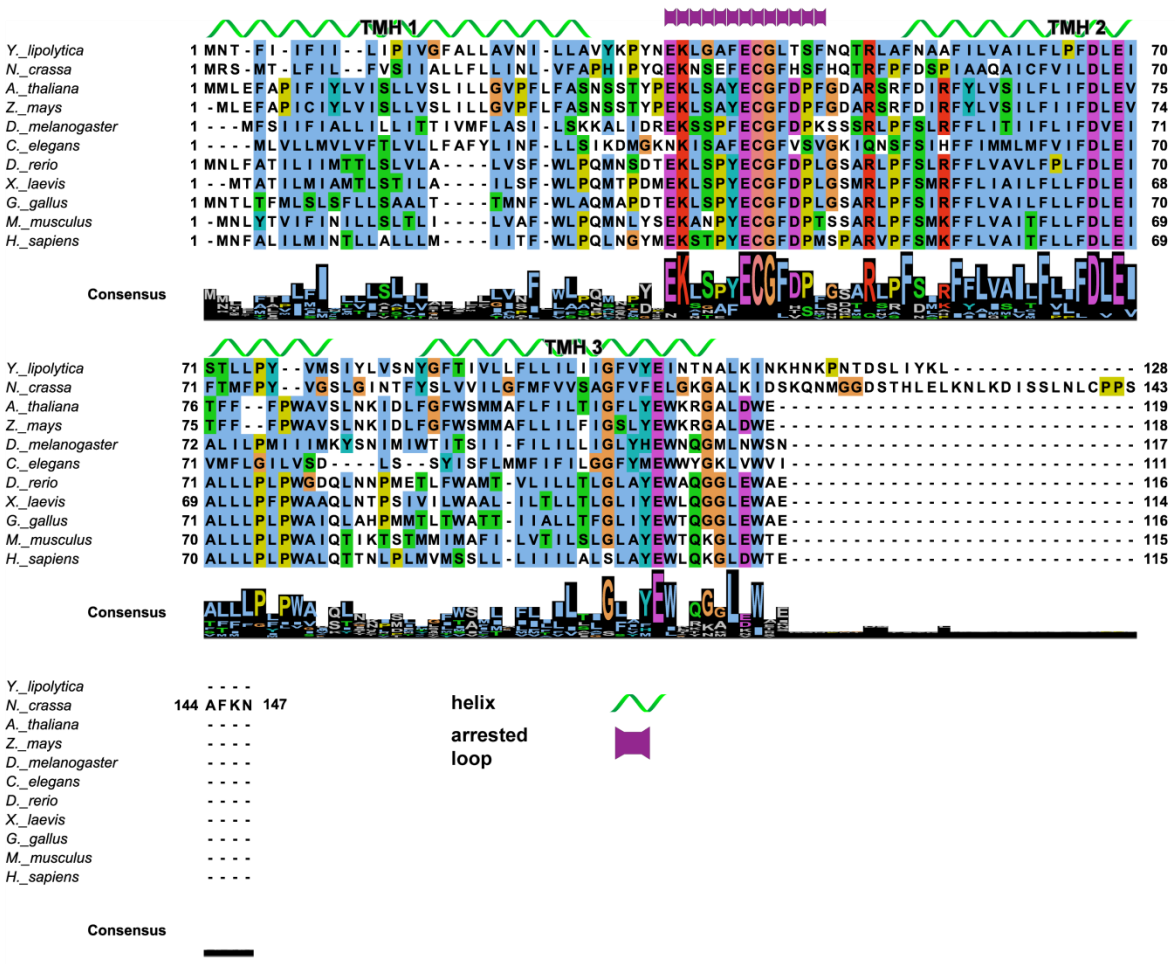

Fig. S11. Alignment of ND3 Sequences. Sequence IDs used in this alignment: P03897 *H. sapiens*, P03899 *M. musculus*, P03900 *X. laevis*, P18930 *D. melanogaster*, P18938 *G. gallus*, Q9MIY3 *D. rerio*, P24895 *C. elegans*, Q35141 *N. crassa*, P92533 *A. thaliana*, Q9B6C7 *Y. lipolytica* and P16265 *Z. mays*. Purple polygons indicate residues of the ND3 loop arrested by NDUFAF1.

Table S1. Complex I content and ubiquinone reductase activity

Strain	dNADH:DBQ[1] [µmol·min^{-1}·mg^{-1}] (%)	NADH:HAR[2] [µmol·min^{-1}·mg^{-1}] (%)
parental	0.6 ± 0.02 (100)	1.2 ± 0.09 (100)
*ndufaf1*Δ	(0)[3]	0.18 ± 0.02 (14)
complementation with *NDUFAF1*	0.63 ± 0.02 (104)	1.02 ± 0.03 (84)
complementation with *NDUFAF1* strep-tag	0.62 ± 0.04 (104)	1.09 ± 0.13 (90)

[1] Inhibitor sensitive dNADH:decylubiquinone oxidoreductase activity was normalized to complex I content.
[2] Content of complex I was assessed as NADH:hexaammineruthenium (III) oxidoreductase activity.
[3] below detection limit

Table S2. Cryo-EM data and model statistics

	Early P_P module assembly intermediate	**Late P_P module assembly intermediate + NDUFAF1 + CIA84**	**Late P_P module assembly intermediate + NDUFAF1**	**Late P_P module assembly intermediate (without assembly factors)**
Data collection and processing				
Electron microscope	Titan Krios G3i	Titan Krios G3i	Titan Krios G3i	Titan Krios G3i
Electron detector	K3 (counting)	K3 (counting)	K3 (counting)	K3 (counting)
Magnification	105,000	105,000	105,000	105,000
Voltage (kV)	300	300	300	300
Total exposure (e^{-}/Å^2)	60	60	60	60
Number of frames	60	60	60	60
Defocus range (μm)	-1.0 to -3.0	-1.0 to -3.0	-1.0 to -3.0	-1.0 to -3.0
Calibrated pixel size (Å)	0.837	0.837	0.837	0.837
Symmetry imposed	C1	C1	C1	C1
Number of micrographs	6,229	6,229	6,229	6,229
Initial particle images (no.)	2,048,808	2,048,808	2,048,808	2,048,808
Final particle images (no.)	376,810	18,279	20,058	220,900
Final resolution (Å)				
At FSC threshold 0.143	3.2	3.2	3.3	3.0
Res. after *DenseMod* (Å)				
At FSC_{ref} threshold 0.5	3.1	3.1	3.2	2.9
Model building and refinement				
Initial models used	7o71			7o71, 7zkq
Model composition				
Protein chains	5			14
Protein residues	1497			2237
Ligands	4			5
R.m.s. deviations				
Bond lengths (Å)	0.27			0.27
Bond angles (°)	0.47			0.47
Ramachandran plot				
Favored (%)	96.96			95.57
Disallowed (%)	0.07			0.21
Validation				
MolProbity score	1.66			1.86
Clashscore	9.08			10.82
Poor rotamers (%)	0.23			0.09

Movie S1. The early P_P module intermediate

Movie S2. The late P_P module intermediate

Movie S3. Pathogenic mutations in tafazzin

Overlay of *Y. lipolytica* tafazzin (lime green) cryo-EM structure with the AlphaFold model of human tafazzin, colored according to pLDDT (predicted Local Distance Difference Test) confidence score. Disease related and conserved residues around the active site are highlighted (magenta). Labels refer to *Y. lipolytica* numbering.

Movie S4. Cardiolipin in complex I

Structure of complex I from *Yarrowia lipolytica* (pdb 6rfr) and bound cardiolipin molecules (shown in yellow).

Movie S5. Structural rearrangements in the late P_P module intermediate upon complex I maturation

Atomic model morph between the late P_P module intermediate and the P_P module in mature complex I (pdb 7o71).